Multitemporal Structure-from-Motion: A Flexible Tool to Cope with Aerial Blocks in Changing Mountain Environment

Nicola Genzano [1], Davide Fugazza [2], Rasoul Eskandari [1], Marco Scaioni [1]
[1] Politecnico Milano, Dept. of Architecture, Built Environment and Construction Engineering (DABC)
Milano, Italy – [nicola.genzano, rasoul.eskandari, marco.scaioni]@polimi.it
[2] Università degli Studi di Milano, Department of Environmental Science and Policy (DESP), Milano, Italy
davide.fugazza@unimi.it

Keywords: Aerial Photogrammetry, Change Detection, Drone Photogrammetry, Ground Control, Monitoring, Structure-from-Motion, UAV/UAS

Abstract

The application of *Structure-from-Motion* (SfM) and *Multi-View-Stereo matching* with aerial images can be successfully used for deriving dense point clouds to analyse changes in the mountain environment, which is characterized by changes due to the action of natural process. The comparison of multiple datasets requires to setup a stable reference system, task that is generally implemented by means of ground control points (GCPs). On the other hand, their positioning may be sometimes difficult in mountains. To cope with this drawback an approach termed as *Multitemporal SfM* (MSfM) is presented: multiple blocks are oriented together within a unique SfM project, where GCPs are used in only one epoch for establishing the absolute datum. Accurate coregistration between different epochs depends on the automatic extraction of tie points in stable areas. To verify the application of MSfM in real cases, this paper presents three case studies where different types of photogrammetric data are adopted, including images from drones and manned aircrafts. Applications to glacier and mountain river erosion are entailed.

1. Motivations

Aerial and satellite optical datasets have been demonstrated to be suitable tools for monitoring changes in the mountain environment, including glaciers, landslides, forests, rivers, and ecosystems (Jombo et al., 2023). Thanks to photogrammetric techniques for image orientation, camera calibration and 3D reconstruction, dense point clouds can be obtained to be used for geomorphological analyses, change detection, volume computation, feature extraction, etc. Aerial manned/unmanned missions may provide high-resolution images for these aims. Missions can be organized on purpose, while online image repositories offer the chance to retrieve data from the past at no or low-cost for the users (Poli et al., 2020). For example, the geoportals "IGN – Remontez le temps" (IGNF, 2024) provide several aerial blocks in the Alpine region of France and Italy.
Consolidated photogrammetric techniques, such as *Structure-from-Motion* (SfM) and *Multi-View-Stereo* (MVS) dense matching can be successfully used to accomplish the 3D reconstruction process based on every type of images (from drones, aircrafts, natively digital or digitized from analogue photos), as proved in previous works (see, e.g., James et al., 2019). New matching methods based on AI-algorithms have been also applied for feature and dense matching between images with strong geometric/radiometric changes, which are typical of the mountain environment (see Maiwald et al., 2023; Morelli et al., 2024). On the other hand, their application is not yet implemented in the routinary processing of photogrammetric blocks.
When the purpose of the study is to compare point clouds (or derived 3D surface models), the stability of the reference system where multi-temporal data sets should be georeferenced is a fundamental prerequisite. While photogrammetry offers all necessary solutions to this goal, many real applications may suffer from the lack/scarcity of ground control. In addition, a good ground control also helps compensate for possible bias in the exterior orientation or in camera calibration, especially with small drones. Practical reasons of critical ground control are:

- the difficult or impossible placement and/or measurement of a sufficient number of well distributed ground control points (GCPs);
- the adopted platform is not equipped with IMU/GNSS sensors for direct orientation;
- the use of archive photos for which ground-control information might not be available; and
- different geodetic reference frames adopted for the measurement of GCPs' coordinates (Barbarella and Fiani, 2013), especially when datasets span over long periods of time.

During different research projects focused on investigating changes in the mountain environment, the authors have realized the need for alternative techniques to replace or to integrate the use of GCPs when comparing multitemporal data sets. In this article the focus is given to the *Multitemporal Structure-from-Motion* (MSfM), which is presented here as a solution to obtain an accurate coregistration between photogrammetric blocks captured at different epochs. While this approach was already presented by the authors to deal with multitemporal data sets of aerial archive photos (Scaioni et al., 2023), here the methodology is reported with the general purpose to align any type of aerial data, including the integration of different data types in the same project (see Sect. 2). Some examples to demonstrate the quality of MSfM in different kinds of mountain environments are shown and discussed in Section 3, while conclusions are presented in Section 4, respectively.

2. Multitemporal Structure-from-Motion

2.1 Georeferencing multitemporal photogrammetric blocks

Structure-from-Motion (SfM) is referred today as the entire automatic procedure for computing the image orientation of a block of images (Granshaw, 2018; James et al., 2019). While at the beginning SfM could be only applied to close-range photos, successive development in processing and computing

techniques extended its application to any types of images, see Barazzetti et al. (2019).

When photogrammetric projects are used for monitoring/detecting changes within time based on the comparison of point clouds (or derived digital elevation models – DEMs; see Lindenbergh and Pietrzyk, 2015) or from *surface feature tracking* (see Luo et al., 2021), more blocks of images are collected at multiple epochs and processed. Georeferencing each block in the same reference system is fundamental to allow the recognition and quantification of meaningful changes.

In general, a block is processed independently from others and georeferenced by means of a set of GCPs measured using GNSS and surveying techniques. After MVS dense matching, a point cloud is obtained to be compared with respect to other datasets.

In the case of aerial blocks based on missions operated with manned aircrafts or drones (see Giordan et al., 2017), GCPs can be identified as *natural* features on the ground or placed on purpose by using suitable *markers* (see examples in Sect. 3). When archive photos are used, the only solution is to identify natural features in the images and to derive their coordinates from *in situ* measurements (when possible) or from geodata (typically digital maps and DEMs). In the case archive photos are used, often the former solution is the only viable, with consequent reduction of the precision of GCP coordinates.

In addition, as reported in Scaioni et al. (2018), when a photogrammetric block is collected in the mountain environment, other problems may influence the quality of GCP measurement (e.g., non-accessible places, bad weather conditions, absence of GNSS positioning services, etc.).

A complete (or at least partial) alternative solution to the use of GCPs is related to direct georeferencing. In the case of manned aerial missions adopting special aircrafts and photogrammetric cameras, the integration with INS/GNSS system for direct georeferencing is today a state-of-the-art solution. Unmanned Aerial Systems (UAS) equipped with RTK/GNSS are becoming quite popular and they may help to solve for georeferencing (Dall'Asta et al., 2019). In both cases, a few GCPs may help to compensate for small biases related to the adopted geodetic *datum*. On the other hand, when using any kinds of archive photos, this solution is not possible unless data collection was operated by means of direct georeferencing technology. But also, in the case this approach was followed, attention should be paid on the coherent selection of the reference frame at each data collection epoch.

In conclusion, the common strategy based on independent georeferencing of each photogrammetric block has some practical drawbacks, which deserve the development of another alternative processing framework.

2.2 Multitemporal SfM (MSfM)

An alternative procedure for handling the orientation of multiple photogrammetric blocks, is to bundle together all of them and to compute the image orientation/camera calibration at the same time, as firstly proposed by Feurer and Vinatier (2018), whose solution was termed as "Time-SIFT." The advantage of this approach is that images from all epochs are aligned together based on tie points matched across images in each block and across different blocks. Ground control is provided by GCPs to be used only for global georeferencing, requiring a quality that may also be at lower accuracy. For example, if one of the adopted photogrammetric blocks is provided with accurate GCPs (e.g., a block captured recently), this could be used for georeferencing all data sets.

Disadvantages and problems may be related to the different quality, resolution, and radiometric content (panchromatic *vs* RGB) of images, and changes in the content. This last aspect is very crucial when dealing with the high mountain environment, where changes may be important.

The implementation proposed in this paper is termed *Multitemporal SfM* (MSfM) and is based on a popular, low-cost software package (Agisoft Metashape Professional) that does not require tailored code development. On the other hand, the same approach is prone to be implemented within other photogrammetric software packages. MSfM works through four main steps:

1. each block is independently processed without considering overlap with other data sets. If available, GCPs (or other types of ground control – e.g., GNSS/IMU or GNSS camera poses) are measured in a "reference" data set to setup the geodetic *datum* in the *bundle-block adjustment* (BBA). In other data sets, a minimum constraint datum can be used (Luhmann et al., 2019). During this phase, each camera is independently self-calibrated;
2. multiple blocks are progressively included in MSfM project to compute the final exterior orientation. The datum established at step (1) is applied again, as well as camera calibration parameters previously estimated;
3. the exterior orientation estimated on the basis on MSfM is adopted to derive a dense point cloud from each original data set based on MVS dense matching; and
4. a final empirical quality assessment is based on the comparison of segmented point clouds inside some well distributed and representative Stable Areas or by measuring some control points. These are selected in locations where no significant changes are expected: on bare rock, on low-vegetated areas, on outcrops, and the like.

Specific problems and related solutions can be applied to each individual project depending on the nature of the adopted platforms and images, as shown in next section through the presentation of three case studies.

3. Applications

Three examples are reported to demonstrate the efficiency of MSfM in practical applications. Each of them copes with a different type of aerial data (photos from archive aerial missions, drone images, mixed datasets) covering various Alpine terrains (glaciers, grass-covered valley with changing riverbed). The ground control has been established based on multiple solutions: precise GNSS measurement of markers or derived from existing maps and DEMs. Table 1 shows the main features of each case study.

3.1 Val Veny glaciers (Case study 1)

3.1.1 Data set presentation: This data set includes archive aerial photos downloaded from the online repository "IGN – Remontez le temps" (IGNF, 2024), which covers the Val Veny area in the Mount Blanc massif, in the Italian region at the border with France. This area includes four important glaciers, as shown in Figure 1. The time extension of these data sets (#6) ranges from 1967-2006. As can be seen in Table 2, aerial blocks in this dataset feature different characteristics, including analogue and digital sensors, radiometric content as well as ground resolution.

Case Study	Id	Location	Data types	#epochs	Ground control
Val Veny glaciers	1	Valle d'Aosta, Italy	Archive aerial photos (PAN, RGB, DAC)	6 (1967-2006)	GCPs measured on digital map/DEM
Forni Glacier	2	Alta Valtellina, Italy	Drones (fixed wing, multicopter), aerial photos	7 (2014-2021)	GCPs measured on site
Rootmos Valley	3	Oeztal, Tyrol, Austria	Drones (fixed wing, multicopter)	3 (2015-2019)	GCPs measured on site

Table 1. Main features of case studies presented in Section 3 (PAN: panchromatic; RGB: colour images; DAC: digital airborne camera; GCP: ground control points; DEM: digital elevation model)

The general purpose of this study is to carry out the analysis of glacier changes over time, to be possibly integrated by older data sets (from the '50s) and satellite high-resolution data in the latest two decades.
Photos collected by analogue cameras were scanned by IGNF with photogrammetric scanners at pixel size of 20 µm. Some datasets are also provided with a calibration certificate (Luhmann et al., 2019) and with approximate camera locations recorded by navigation GNSS sensors. Due to the lack of GCPs in all delivered data sets, a set of seven features have been located on buildings and rocks (see Fig. 1). Their coordinate in the Italian mapping grid have been derived from a geoportal and from a DEM for East-North coordinates and elevation, respectively. These GCPs have been used in BBA only to globally setup the geodetic *datum*, since their accuracy was in the order of ±10 m.

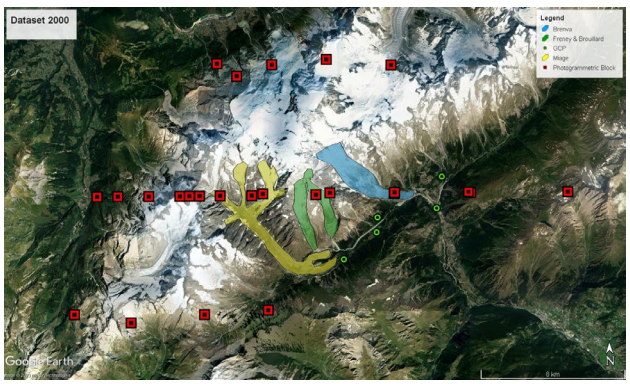

Figure 1. Case study 1: The area of Val Veny (Italy) in the Mount Blanc Massif with localization of four glaciers to be investigated, GCPs, and photos from Block 2000.

3.1.2 Data processing. The processing pipeline described in Subsection 2.2 for MSfM has been applied to the aerial blocks in Table 1. More details can be found in Scaioni et al. (2023). A set of seven GCPs has been initially used for georeferencing all blocks in the reference frame RDN 2008.0 / UTM32N. Images have been pre-processed to improve the image quality, see Malekian et al. (2023). Tailored masks designed per each camera have been applied to exclude the outer frame for digitized analogue photos.
Agisoft Metashape Professional® ver. 2.1.0 (AMP) has been used for the independent exterior orientation (EO) of selected blocks. A minimum constraint datum has been used (see Luhmann et al., 2019) to compute the EO per each block.

Time	#Images (type)	Camera Model (focal length)	Avg. flying altitude [m a.s.l.]
2006 (Aug 23-Sept 5)	78 (RGB)	DAC IGNF (60 mm)	5,540
2001 (Aug 1-13)	73 (RGB)	Zeiss RMKTOP15 (150 mm)	4,780
2000 (Jun 23-Aug 1)	25 (RGB)	Zeiss RMKTOP15 (150)	5,540
1996 (Jul 3-Aug 4)	35 (RGB)	Zeiss RMKTOP15 (150 mm)	5,020
1988 (Jul 26)	23 (PAN)	Leica RC10 (150 mm)	6,150
1967 (Oct 11-12)	24 (PAN)	Leica RC10 (150 mm)	6,350

Table 2. Case study 1: Main features of photogrammetric data sets from IGNF online repository.

Exterior orientation (EO) has been computed on full-resolution data ("Highest" quality level). Almost all photos in each block could be oriented except 3% of their total number. BBA has been also used to compute the inner orientation of the adopted aerial cameras. Those parameters that could be derived from available calibration certificates have been introduced as fixed or approximate values. When present, fiducial marks have not been considered to establish the "photo coordinate system," but point measurement in image space has been done by using the "pixel coordinate system" directly. Misalignment errors during scanning could be compensated for shifting E_o and N_o object coordinates of the perspective centres during BBA. Residuals on tie points (TPs) in image space have been positively checked for the type and quality of the adopted images.
After independent EO and camera calibration, all blocks have been processed together using MSfM in AMP. To compute final EO, each block has been transformed in the same reference system based on seven GCPs. Conformal transformations have been adopted to this purpose and to fix the approximate scales. On the other hand, Data set 2000 has been used to establish the datum in MSfM. The measurement of GCPs has been also extended to some images from other datasets where they could be clearly identified and manually measured. MSfM has been applied to all available images from six blocks in Table 2, resulting in the successful estimate of the EO. A total number of 103,259 tie points (average 2.92 rays/point) has been obtained, to be used as input for the final BBA. The average number of TPs per image ranges from 1,928 (in Data set 1988) to 3,903 (in Data set 2006). Average residuals on image coordinates always are at subpixel values, except for Data set 1988 (1.54 pixels) and Data set 2001 (1.12 pixels). Root Mean Squared Errors (RMSEs) of residuals on the object coordinates of GCPs result as 7.08 m in position and 5.80 m in elevation, as compliant with the accuracy of GCP coordinates, which has been adopted for properly weighting these observations in the BBA.

3.1.3 Quality assessment. Since the purpose of this project is to derive point clouds at different epochs for computing changes on the Alpine glaciers in Val Veny, the quality assessment is focused on the evaluation of point cloud registration errors. This is the only possible method to be applied in a such case, due to the difficulty of detecting stable independent check points within time, as proposed in the literature (Eltner et al., 2015). To this purpose, a dense point cloud has been generated from each data set in AMP at quality level "High." The EO estimated from MSfM has been used for dense matching. Point clouds have been imported in the open-source software CloudCompare (CC) Ver. 2.12.4 "Kyiv" (www.Cloudcompare.org). After filtering out duplicated and isolated points, five Stable Areas (SAs) have been selected for quality assessment.

Segmented point clouds in SAs have been compared in a pairwise manner from different epochs by using *Multi-scale Model to Model* (M3C2) distance, see Lague et al. (2013). Results of comparisons between consecutive epochs are reported in Table 3, that shows also the outcomes based on the independent SfM per each epoch, and a third approach where MSfM is followed by a refinement of point cloud registration. This refinement has been applied based on the *Iterative Closest Point* algorithm (ICP – see Pomerleau et al., 2013) in SAs, as described in Scaioni et al. (2023). As can be seen in Table 3, MSfM allows to reduce the absolute value of the mean of M3C2 distances between consecutive point clouds. An even better improvement can be noticed about the standard deviation of M3C2 distances. The effect of applying the ICP refinement is to bring close to zero the mean distances as well as to further mitigate the standard deviations and the RMSE, consequently. These results demonstrate a residual bias left after MSfM, that is significantly smaller than the residual bias after independent SfM.

Epochs	Statistics	Single SfM [m]	MSfM [m]	MSfM + ICP [m]
1967 - 1988	*mean*	-1.31	-0.82	0.02
	std.dev.	3.04	1.25	1.09
	RMSE	3.31	1.49	1.09
1988 - 1996	*mean*	0.67	-0.11	-0.17
	std.dev.	3.10	1.99	1.87
	RMSE	3.18	1.99	1.88
1996 - 2000	*mean*	-1.82	-0.46	-0.22
	std.dev.	3.82	2.37	2.07
	RMSE	4.47	2.41	2.08
2000 - 2001	*mean*	1.61	0.18	0.05
	std.dev.	4.39	0.91	0.72
	RMSE	4.48	0.93	0.72
2001 - 2006	*mean*	0.31	0.19	0.08
	std.dev.	3.80	0.71	0.67
	RMSE	3.81	0.73	0.67

Table 1. Case study 1: Statistics on *Multi-scale Model to Model* (M3C2) distances for the comparison of point clouds in Stable Areas (SAs) according to three processing pipelines: (1) *independent SfM* (Structure-from-Motion) per each data set; (2) *Multitemporal SfM* (MSfM); and (3) MSfM followed by *Iterative Closest Point* (ICP) refinement.

3.2 Forni Glacier: drone and aerial photos (Case study 2)

3.2.1 Data set presentation. The second case study presented here is related to the investigation of Forni Glacier, in the Ortles-Cevedale group (Southern Rhaetian Alps, Italy). The glacier is one of the largest in the country (in 2007 it covered an area of 11.34 km^2 – see Smiraglia et al., 2016) and in the latest decades has undergone a fast retreat. For this reason, starting in 2014, some research groups have started to carry out measurement campaigns based on the use of drone-photogrammetry on the glacier terminus, which is located at approx. 2500 m a.s.l. (see Fugazza et al., 2018; Di Rita et al., 2020). The purpose of these campaigns was to evaluate the volume change due to melting in correspondence of the terminus as well as to detect the presence of local collapsing processes, see Scaioni et al. (2017).
The study area presents advantages such as reduced inclinations favourable to drone photogrammetry and easy access for the installation of GCPs. On the other hand, the glacier is in the Stelvio National Park, preventing the installation of permanent markers. Consequently, in correspondence of any campaign a set of markers was deploid on the glacier/periglacier areas and measured thanks to GNSS-RTK and theodolite techniques.

In Table 4 available data from fixed-wing and multicopter drones are listed. Due to the poor air density, the time available per each flight was in general limited to 15-25 minutes. For this reason, each block comes from the composition of more flight missions. In addition, meteorological conditions resulted in splitting missions in more days to exploit time slots with good wheather. The original data sets were subsampled in order to keep only those images depicting the glacier terminus. As can be seen in Figure 2, the original 4,142 images were reduced to 2,420 total images (42% of images discarded). This selection allowed to focus on the overlapping images whilst reducing the processing time.

Time	Drone type / camera	#images (original/ selected)	Avg. relative flying altitude [m] / GSD [cm]	# GCPs
2014 (Aug)	fixed wing SwingletCam SenseFly / RGB1	86/29	380 / 12	n.a.
2016 (Aug-Sept)	customized quadcopter / RGB2	291/210	184 / 6	8
2017 (Oct)		161/161	145 / 6	5
2018 (Aug)		299/271	102 / 6	7
2019 (Oct)	manned aircraft / DAC1	12/12	4700 / 20	n.a.
2020 (Aug)	quadcopter DJI Phantom 4 / RGB3	1489/746	160 / 5	n.a.
2021 (Aug)		1817/1003	160 / 5	n.a.

Table 4. Case study 2: Main features of photogrammetric data sets (GSD: ground sampling distance). The following acronyms are used for the adopted cameras (in brackets: camera name, sensor size, focal length): RGB1 (Canon IXUS 127 HS: 16 Mpixels, 4.3 mm); RGB2 (Canon PowerShot ELPH 320 HS: 16 Mpixels, 4.3 mm); DAC1 (digital aerial camera); RGB3 (DJI FC6310R: 20.0 Mpixels, 16 mm).

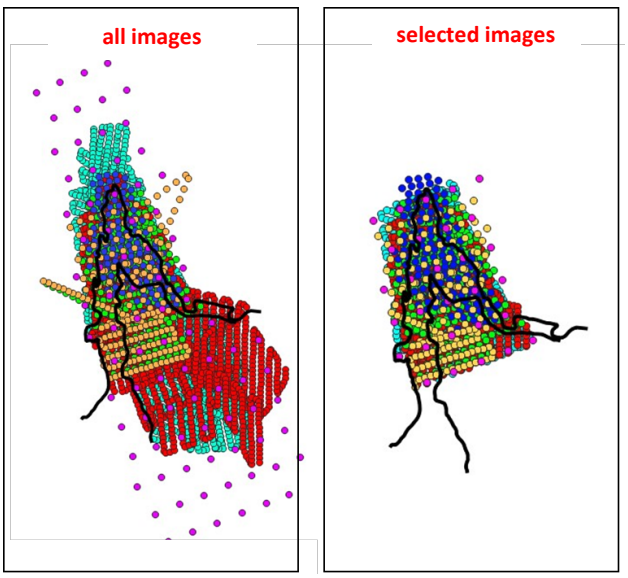

Figure 2. Case study 2: Location of all collected (on the left) and selected (on the right) images (for UAV blocks). The black profile reports the extension of the Forni Glacier terminus in correspondence of the oldest (2014) and the latest (2021) epochs, respectively.

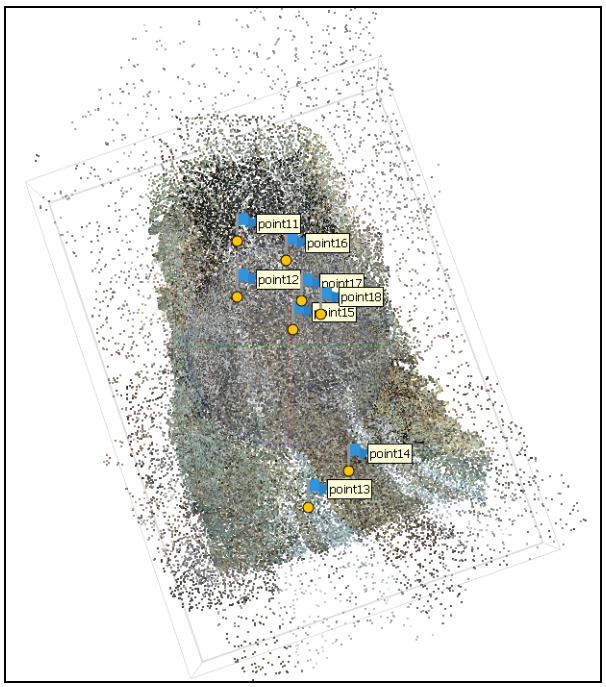

Figure 3. Case study 2: Sparse point cloud made up of tie points extracted with MSfM. Blue flags represent GCPs from Block 2016.

One photogrammetric block from aerial missions for topographic mapping are also available to cover 2019, when UAV missions were not accomplished. On the other hand, this flight features a completely different photo scale.

3.2.2 Data processing. The processing pipeline described in Subsection 2.2 for MSfM has been applied to the aerial blocks in Table 4. GCPs in Block 2016 (#8 – see Fig. 3) have been measured in relevant images and used for georeferencing all “selected” images (#2418) in the Italian reference frame RDN 2008.0/UTM32N. Due to the large total number of photos, image orientation (including camera self-calibration) has been carried out on half-resolution images corresponding to “High” quality level in AMP. After BBA, 4.6% of images could not be oriented, yielding 125,343 TPs (Fig. 3). RMSE of residuals on GCPs turned out to be 9.1 cm in object space and 0.65 pixels in images space, respectively.
These results do not include Block 2019 collected using an aerial digital camera. Due to the large difference in scale w.r.t. images from drones, the extraction of common inter-epoch TPs with this block was not successful.

3.2.3 Quality assessment. The quality assessment has been carried out as for Case study 1, since also in this case the purpose of data collection is to compute volume change of the glacier terminus. A dense point cloud has been generated from each data set in AMP at quality level “High.” Point clouds have been imported in the open-source software CloudCompare (CC) Ver. 2.12.4 “Kyiv”.
After filtering out duplicated and isolated points, three Stable Areas (SAs) have been selected for pairwise comparison by using M3C2 (Fig. 4).
Results are reported in Table 5 in terms of statistics on M3C2 distances, weighted based on the number of points per each SA. In the same table, corresponding results from processing of single epochs based on independent SfM and available GCPs are reported as well. For this reason, only two comparisons (2016-2017 and 2017-2018) could be possible w.r.t. MSfM. As can be seen, mean values of distances are close to zero per each comparison based on EO parameters computed by MSfM. On the other hand, mean values for independent SfM show very large errors, which are probably due to mistakes in measurement of GCPs in the field. This hypothesis is supported by the fact the standard deviations do not differ too much between independent SfM and MSfM. On the other hand, standard deviations computed on comparisons including “Block 2017” and successive ones feature very small standard deviations, probably because of the better quality of the images.

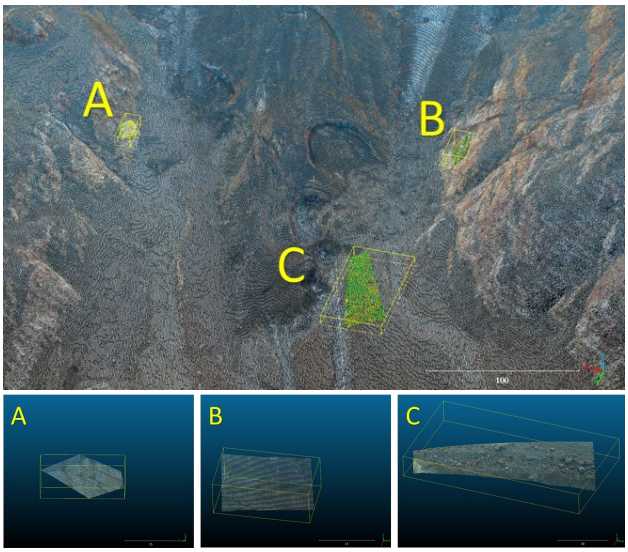

Figure 4. Case study 2: Location of three Stable Areas (SA) outside Forni Glacier to be used for quality assessment (at the top); point clouds segmented in each SA (at the bottom).

Epochs	Statistics on M3C2 differences	Indep. SfM [m]	MSfM [m]
2014 - 2016	*Mean*	n.a.	0.02
	std.dev.	n.a.	0.13
	RMSE	n.a.	0.13
2016 - 2017	*mean*	-0.56	0.00
	std.dev.	0.17	0.16
	RMSE	0.59	0.16
2017 - 2018	*mean*	1.59	0.01
	std.dev.	0.33	0.04
	RMSE	1.62	0.04
2018 - 2020	*mean*	n.a.	-0.03
	std.dev.	n.a.	0.04
	RMSE	n.a.	0.05
2020 - 2021	*mean*	n.a.	-0.01
	std.dev.	n.a.	0.02
	RMSE	n.a.	0.02

Table 5. Case study 2: Statistics M3C2 distances after comparison of point clouds in three SAs according to two processing pipelines: (1) independent SfM; (2) MSfM.

3.3 Rotmoos Valley (Case study 3)

3.3.1 Data set presentation. This case study was developed during the first three editions (2015, 2017, 2019) of the ISPRS Summer School of Alpine Research in Obergurgl, Austria (Rutzinger et al., 2020). The area of interest of this ongoing study is the foreland of the Rotmoos glacier, located near the Central Alpine Ridge. Several missions flown using fixed-wing

and multicopter drones are available (see Table 6). The purpose of these missions was to derive point clouds useful to analyse the effect of river erosion between multitemporal campaigns, see Backes et al. (2020). At each epoch, some markers were positioned and measured by GNSS and theodolite to be used as GCPs.
In 2015 a single block was collected under intense windy conditions by the Austrian Research Centre for Forests (BFW), see Rutzinger et al. (2016). The flight was driven by onboard navigation-grade GNSS, but no geotags were available for the images. Markers (GCPs) were measured using RTK GNSS with respect to a local master station, then georeferenced in the national network. A still camera installed on a fixed-wing drone was adopted for image acquisition.
In 2017 more data sets were collected (Rutzinger et al., 2018), but here we limited to exploit a block from the same drone and camera adopted in 2015. Markers were positioned and measured by GNSS to be used as GCPs; no geotags were recorded.
In 2019 two main UAS platforms were used (Backes et al., 2020). In this study, some photogrammetric blocks collected using a DJI Phantom 4 were considered. These sub-blocks include nadir images (70% forward and 60% side overlap), cross-strips, and oblique images. Geotags from onboard GNSS are available. A set of 11 markers were installed and measured with GNSS and theodolite to be used as GCPs, but not all of them were visible in all sub-blocks (see Table 6).

Time	Drone type / camera	# images	Avg. relative flying altitude [m] / GSD [cm]	# GCPs
2015 (July)	fixed wing / RGB4	74	100 / 2.9	6
2017 (July)		254	130 /3.0	10
2019 (June)	quadcopter DJI Phantom4 / RGB5	224 (nadir)	77 / 2.0	11
		27 (cross)	97 / 2.5	4
		108 (oblique)	43 / 1.1	4

Table 6. Case study 3: Main features of photogrammetric data sets collected by drones. The following acronyms are used for adopted cameras (in brackets: camera name, sensor size, focal length): RGB4 (Sony NEX-5: 15.1 Mpixels, 16 mm); RGB5 (DJI FC5310: 20.0 Mpixels, 8.8 mm).

3.3.2 Data processing. In Backes et al. (2020) the photogrammetric processing of individual blocks is reported based on independent SfM per each epoch and corresponding sets of GCPs. Due to the presence of some errors in the definition of the geodetic *datum* at different epochs, the direct comparison of point clouds obtained from MVS dense matching was not possible. For this reason, this case could demonstrate whether the application of MSfM is able to overcome situations where a stable reference frame is not available.
The image orientation and camera calibration based on MSfM has been followed the standard process described in Subsection 2.2. In a first stage, all blocks have been independently processed based on SfM to estimate EO and camera calibration parameters. This task has been carried out since some Blocks 2015 and 2017 were not provided with geotags to speed up the computation of MSfM. First a "free-net" BBA has been computed in AMP (ver. 2.1.1) per each epoch. Different options for the selection of Additional Parameters to estimate have been tried with no significant changes. GCPs positioned at each epoch were manually measured in images and used with their corresponding ground coordinates to merge all blocks. The set of 11 GCPs measured in 2019 has been selected to define the ground reference system for the final MSfM. The image coordinates of these markers were measured on the nadir photos from DJI Phantom 4 Block 2019.
A total of 441,514 TPs have been measured, leading to the EO of all 687 images included in the MSfM project. Looking at the quality/number of TPs in different blocks, the better performance has resulted for Block 2019 (RMSE of residuals in image space 0.42 pixels and number of TPs between 3,500 and 5,600 per photo). In the case of other blocks, RMSEs of residuals in image space have resulted as 0.75/0.94 pixels for Blocks 2015 and 2017, respectively. A larger number of TPs per image has been found in Block 2017 (in the range 1,700-4,300 TPs per photo) than in Block 2015 (750-2,300 TPs per photo). RMSEs of residuals on 11 GCPs has resulted 3.1 cm in 3D object coordinates and 0.30 pixels in image space.

3.3.3 *Quality assessment.* The purpose of collecting multiple blocks in Rootmos Valley is to detect changes due to river erosion. Consequently, some Stable Areas (SAs) could have been selected to check for misalignment errors as in the previous study cases. On the other hand, as can be seen in Fig. 5, the differences on the terrain covered by blocks in Case study 3 are quite large. The identification of SAs should be on grass or riverbed regions. For this motivation, the comparison between the EO computed for each block during BBA of MSfM has been based on the localization and measurement of 20 check points (CPs). These have been identified in the entire region overlapped among multiple epochs, even though not all of them could be measured in all data sets. 3D object coordinates of CPs have been computed based on the EO of each block and compared in a pairwise manner. Table 7 shows some statistics on the computed differences. When comparing Epochs 2017 and 2019, the results are quite satisfying, even though the RMSE for the difference in elevation is 19 cm.

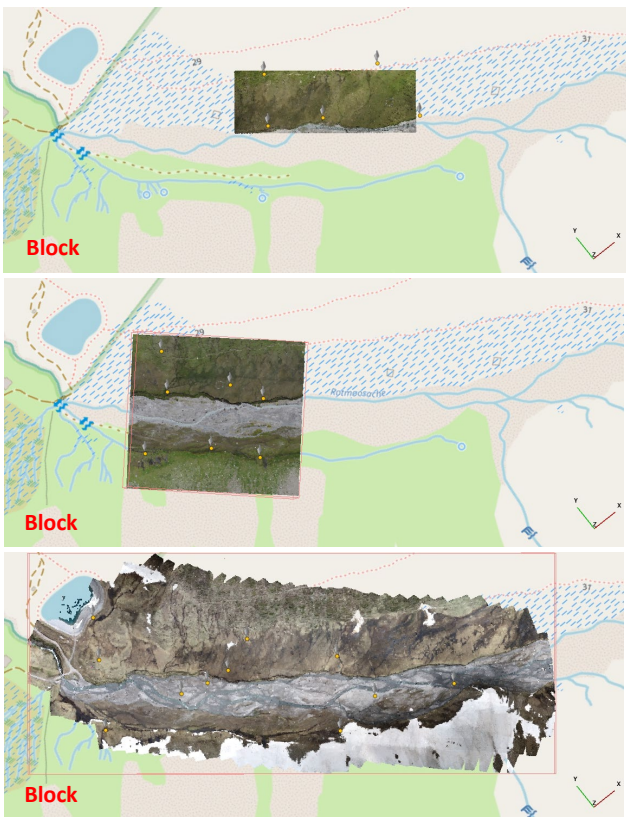

Figure 5. Case study 3: Orthographic view of point clouds obtained from Blocks 2015, 2017, 2019. Yellow circles give the location of GCPs measured during each campaign.

Epochs	# CPs	Statistics on CP differences	ΔE [m]	ΔN [m]	ΔH [m]
2015 - 2017	8	*mean*	0.00	-0.27	0.69
		std.dev.	0.14	0.26	0.75
		RMSE	0.14	0.37	1.03
2017 - 2019	16	*mean*	-0.02	0.02	0.11
		std.dev.	0.09	0.06	0.15
		RMSE	0.09	0.06	0.19
2015 - 2019	8	*mean*	-0.05	-0.24	0.90
		std.dev.	0.15	0.29	0.81
		RMSE	0.16	0.38	1.21

Table 7. Case study 3: Statistics on the differences between control points (CPs) object coordinates.

On the other hand, when Epoch 2015 is involved, the results are very large and not acceptable. Elevations and North coordinates report the worse outcomes, which are due either to a bias (mean) and to a scattering (standard deviation), sharing a similar size.

3.4 Discussion

In this section three application of MSfM are reported with the purpose of understanding its applicability to real case studies in the mountain environment. Study cases 1 and 2 concern Alpine glacier monitoring, while Case study 3 is related to a mountain valley partially covered by grass and hosting a riverbed with active fluvial erosion.

In both cases concerning glaciers, despite of the big changes in the multitemporal scenes, MSfM was successfully applied. This evaluation comes from two main reasons: (1) the effective EO of almost all images, with a few exception in term of percentage of the total number of photos; (2) the positive results of quality assessment, which provided a sufficient precision according to the purpose of each case study and the size of changes to be detected.

In Case study 3, MSfM could not be retain successful, in particular as far as the oldest photogrammetric block (2015) was concerned. The possible reasons of this failure may be addressed in three points: (1) a poor overlap between drone missions at different epochs, especially with the one on 2015; (2) the presence of grass and eroded riverbed in the overlapping regions, resulting in problems with the extraction of inter-epoch TPs; and (3) the poor geometry of Block 2015 due to the irregular flight caused by the wind.

To understand in advance whether MSfM could work, an analysis on the presence of sufficient areas to detect inter-epoch TPs may be useful. In this direction, a preliminary test on small subsets of 3-4 overlapping photos per epoch, taken in some representative spots of the Region-of-Interest, could be useful to evaluate the applicability of MSfM for the whole block.

MSfM is a valid solution for coregistration of several blocks of images collected at different times when ground control is not available. Case study 1, where historical archive photos were used, demonstrated that data covering a time span of a few decades can be processed as well. The presence of some residual bias in coregistration may require a final refinement based on algorithms for point cloud registration (e.g., ICP). On the other hand, in absence of ground control, the unique alternative to MSfM is to apply such algorithms on point clouds that have been generated from independent SfM projects. In this study we have not evaluated which solution is more suitable. The analysis of processing time would be necessary to this end, but this strictly depends on the adopted hardware. A more detailed analysis of computational burden is planned in the future.

4. Conclusions

In the paper an approach for computing the contemporary exterior orientation of multiple blocks of aerial images was presented. Thanks to the capability of dealing with data sets collected at different times, it is termed *Multitemporal Structure-from-Motion* (MSfM). The implementation of this method is carried out through a popular photogrammetric software package for SfM (Agisoft Metashape Professional®) without development of specific code. Consequently, any operator provided with this package may apply MSfM for her/his projects.

The specific aim of this paper is to prove the effectiveness of MSfM in three real applications in the mountain environment, which is typically affected by important changes within time. Two cases involving glacier monitoring projects, one afforded on the basis of archive aerial photos, and another based on drone images, were successfully processed. Residual coregistration errors evaluated in stable areas were compliant with the expectation of each project. A third case concerning the orientation of three blocks from drone photogrammetry flown over an Alpine valley affected by river erosion was not successful. As discussed in Subsection 3.4 this failure may be motivated by the absence of stable areas between multiple epochs and by a not proper block geometry.

New applications to extended data sets and other types of data (e.g., multispectral images from drone) are envisaged for the future. On the other hand, more attention to new algorithm for extracting corresponding features based on Deep Learning techniques will be paid.

Acknowledgements

The authors would like to acknowledge the National Geographic and Forestry Institute of France (IGNF) for delivering archive photos adopted in Case study 1; the University of Milano, the University of Rome "La Sapienza," Leica Geosystems, and AGEA (Agenzia per le Erogazioni in Agricoltura, Italy) for the aerial blocks in Case study 2; and the organizers and participants to the ISPRS Summer School of Alpine Research in Obergurgl, the Austrian Research Centre for Forests (BFW), Riegl Laser Measurement Systems GmbH, and the University of Innsbruck for data collection in Case study 3. Acknowledgements also go to the developers of CloudCompare open-source software we used in this research.

References

Backes, D., Smigaj, M., Schimka, M., Zahs, V., Grznárová, A., Scaioni, M., 2020. River Morphology Monitoring of a Small-Scale Alpine Riverbed Using Drone Photogrammetry and LIDAR. *Int. Arch. Photogramm. Remote Sens. Spatial Inf. Sci.*, XLIII/B2-2020, 1017-1024. doi.org/10.5194/isprs-archives-XLIII-B2-2020-1017-2020.

Barazzetti, L., Gianinetto, M., Scaioni, M., 2020. Automatic Processing of Many Images for 2D/3D Modelling. In: B. Daniotti et al. (Eds.), *Digital Transformation of the Design, Construction and Management Processes of the Built Environment,* Research for Development, SpringerOpen, Cham, 355-364. doi.org/10.1007/978-3-030-33570-0_32.

Barbarella, M., Fiani, M., 2013. Monitoring of large landslides by Terrestrial Laser Scanning techniques: field data collection and processing. *Eur. J. Remote Sens.* 46(1), 126-151. doi.org/10.5721/EuJRS20134608.

Dall'Asta, E., Forlani, G., Roncella, R., Santise, M., Diotri, F., Morra di Cella, U., 2027. Unmanned Aerial Systems and DSM

matching for rock glacier monitoring. *ISPRS J. Photogramm. Remote Sens.*, 127, 102-114. doi.org/ 10.1016/j.isprsjprs.2016.10.003.

Di Rita, M., Fugazza, D., Belloni, V., Diolaiuti, G., Scaioni, M., Crespi, M., 2020. Glacier Volume Change Monitoring from UAV Observations: Issues and Potentials of State-of-the-Art Techniques. *Int. Arch. Photogramm. Remote Sens. Spatial Inf. Sci.*, XLIII/B2-2020, 1041-1048. doi.org/10.5194/isprs-archives-XLIII-B2-2020-1041-2020.

Eltner, A., Kaiser, A., Castillo, C., Rock, G., Neugirg, F., Abellán, A., 2016. Image-based surface reconstruction in geomorphometry – merits, limits and developments. *Earth Surf. Dyn.*, 4, 359-389. doi.org/10.5194/esurf-4-359-2016.

Feurer, D., Vinatier, F., 2018. Joining multi-epoch archival aerial images in a single SfM block allows 3-D change detection with almost exclusively image information. *ISPRS J. Photogramm. Remote Sens.*, 146, 495-506. doi.org/10.1016/j.isprsjprs.2018.10.016.

Fugazza, D., Scaioni, M., Corti, M., D'Agata, C., Azzoni, R.S., Cernuschi, M., Smiraglia, C., Diolaiuti, G.A., 2018. Combination of UAV and terrestrial photogrammetry to assess rapid glacier evolution and map glacier hazards. *Nat. Haz. Earth Sys. Sci.*, 18, 1055-1071. doi.org/10.5194/nhess-18-1055-2018.

Giordan, D., Manconi, A., Remondino, F., Nex, F, 2017. Use of unmanned aerial vehicles in monitoring application and management of natural hazards. *Geomatics. Nat. Haz. Risk*, 8, 1-4. doi.org/10.1080/19475705.2017.1315619.

Granshaw, S.I., 2018. Structure from motion: Origins and originality. *Photogramm. Rec.*, 33, 6-10. doi.org/ 10.1111/phor.12237.

James, M.R., Chandler, J.H., Eltner, A., Fraser, C., Miller, P.E., Mills, J.P., Noble, T., Robson, S., Lane, S.N., 2019. Guidelines on the use of structure-from-motion photogrammetry in geomorphic research. *Earth Surf. Process. Landforms*, 44, 2081-2084. doi.org/10.1002/esp.4637.

Jombo, S., Abd Elbasit, M.A.M., Gumbo, A.D., Nethengwe, N.S., 2023. Remote Sensing Application in Mountainous Environments: A Bibliographic Analysis. *Int. J. Environ. Res. Public Health*, 20(4), paper No. 3538, doi.org/ 10.3390/ijerph20043538.

IGNF (National Geographic and Forestry Institute of France), Geoportal "IGN – Remontez le temps." remonterletemps.ign.fr/ (30 April 2024).

Lague, D., Brodu, N., Leroux, J., 2013. Accurate 3D comparison of complex topography with terrestrial laser scanner: Application to the Rangitikei canyon (N-Z). *ISPRS J. Photogramm. Remote Sens.*, 82, 10-26. doi.org/ 10.1016/j.isprsjprs.2013.04.009.

Lindenbergh, R., Pietrzyk, P., 2015. Change detection and deformation analysis using static and mobile laser scanning. *Appl. Geomatics*, 7, 65-74. doi.org/10.1007/s12518-014-0151-y.

Luhmann, T., Robson, S., Kyle, S., Boehm, J., 2019. *Close-range photogrammetry and 3D imaging*. Walter de Gruyter, Berlin.

Luo, S., Cheng, Y., Li, Z., Wang, Y., Wang, K., Wang, X., Qiao, G., Ye, W., Li, Y., Xia, M., Yuan, X., Tian, Y., Tong, X., Li, R., 2021. Ice Flow Velocity Mapping in East Antarctica using Historical Images from 1960s to 1980s: Recent Progress. *Int. Arch. Photogramm. Remote Sens. Spatial Inf. Sci.*, XLIII/B3-2021, 491-496. doi.org/10.5194/isprs-archives-XLIII-B3-2021-491-2021, 2021.

Maiwald, F., Feurer, D., Eltner, A., 2023. Solving photogrammetric cold cases using AI-based image matching: New potential for monitoring the past with historical aerial images. *ISPRS J. Photogramm. Remote Sens.*, 206, 184-200. doi.org/10.1016/j.isprsjprs.2023.11.008.

Malekian, A., Fugazza, D., Scaioni, M., 2023. Photogrammetric Reconstruction and Multi-temporal Comparison of Brenva Glacier (Italy) from Archive Photos. *ISPRS Ann. Photogramm. Remote Sens. Spatial Inf. Sci.*, X/4-W1, 459-466. doi.org/10.5194/isprs-annals-X-4-W1-2022-459-2023.

Morelli, L., Ioli, F., Maiwald, F., Mazzacca, G., Menna, F., Remondino, F., 2024. Deep-Image-Matching: A Toolbox for Multiview Image Matching of Complex Scenarios. *Int. Arch. Photogramm. Remote Sens. Spatial Inf. Sci.*, XLVIII-2/W4-2024, 309-316. doi.org/10.5194/isprs-archives-XLVIII-2-W4-2024-309-2024.

Poli, D., Casarotto, C., Strudl, M., Bollmann, E., Moe, K., Legat, K., 2020. Use of Historical Aerial Images for 3D Modelling of Glaciers in the Province of Trento. *Int. Arch. Photogramm. Remote Sens. Spat. Inf. Sci.*, 43/B2, 1151-1158. doi.org/10.5194/isprs-archives-XLIII-B2-2020-1151-2020.

Pomerleau, F., Colas, F., Siegwart, R., Magnenat, S., 2013. Comparing ICP variants on real-world data sets. *Autonom. Robots*, 34, 133-148. doi.org/10.1007/s10514-013-9327-2.
Rutzinger, M., Höfle, B., Lindenbergh, R., Oude Elberink, S.,

Pirotti, F., Sailer, R., Scaioni, M., Stötter, J., Wujanz, D., 2016. Close-Range Sensing Techniques in Alpine Terrain. *ISPRS Ann. Photogramm. Remote Sens. Spatial Inf. Sci.*, III/6, 15-22. doi.org/10.5194/isprs-annals-III-6-15-2016.

Rutzinger, M., Bremer, M., Höfle, B., Hämmerle, M., Lindenbergh, R., Oude Elberink, S., Pirotti, F., Scaioni, M., Wujanz, D., Zieher, T., 2018. Training in Innovative Technologies for Close-Range Sensing in Alpine Terrain. *ISPRS Ann. Photogramm. Remote Sens. Spatial Inf. Sci.*, IV/2, 239-246. doi.org/10.5194/isprs-annals-IV-2-239-2018.

Rutzinger, M., Anders, K., Bremer, M., Höfle, B., Lindenbergh, R., Oude Elberink, S., Pirotti, F., Scaioni, M., Zieher, T., 2020. Training in Innovative Technologies for Close-Range Sensing in Alpine Terrain – 3rd Edition. *Int. Arch. Photogramm. Remote Sens. Spatial Inf. Sci.*, Vol. XLIII, Part B5-2020: 243–250.

Scaioni, M., Corti, M., Diolaiuti, G., Fugazza, D., Cernuschi, M., 2017. Local and General Monitoring of Forni Glacier (Italian Alps) Using Multi-Platform Structure-From-Motion Photogrammetry. *Int. Arch. Photogramm. Remote Sens. Spatial Inf. Sci.*, XLII/2-W7, 1547-1554. doi.org/ 10.5194/isprs-archives-XLII-2-W7-1547-2017.

Scaioni, M., Crippa, J., Corti, M., Barazzetti, L., Fugazza, D., Azzoni, R., Cernuschi, M., Diolaiuti, G.A., 2018. Technical Aspects Related to the Application of SfM Photogrammetry in High Mountain. *Int. Arch. Photogramm. Remote Sens. Spatial Inf. Sci.*, XLII/2, 1029-1036. doi.org/10.5194/isprs-archives-XLII-2-1029-2018.

Scaioni, M., Malekian, A., Fugazza, D., 2023. Techniques or Comparing Multi-Temporal Archive Aerial Imagery for Glacier Monitoring with Poor Ground Control. *Int. Arch. Photogramm. Remote Sens. Spatial Inf. Sci.*, XLVIII/M-1-2023, 293-300. doi.org/10.5194/isprs-archives-XLVIII-M-1-2023-293-2023.

Smiraglia, C., Diolaiuti, G., Azzoni, R.S., D'Agata, C., Maragno, D., 2016. *The New Italian Glacier Inventory – Revision 2016*. EvK2CNR, Bergamo.